Effect of smectic polymers on cholesteric liquid crystals

Zhaofei Zheng [1,*] and Francesca Serra [1,2,†]

[1] *William H. Miller III Department of Physics and Astronomy, Johns Hopkins University, Baltimore 21218, USA*

[2] *Department of Physics, Chemistry and Pharmacy, University of Southern Denmark, 5230 Odense, Denmark*

(Received 24 April 2024; accepted 16 September 2024; published 14 November 2024)

Composite materials made of polymers and liquid crystals have been widely employed in smart windows, optical filters, and bistable displays. However, it is often difficult to decipher the role of the polymer network architecture on the alignment and the texture of liquid crystals. In this study, we use a simple model system where a small amount of polymerizable liquid crystalline monomer is mixed in a liquid crystal that exhibits both a smectic phase and a cholesteric phase with a large helical pitch. By cross-linking the monomer in the smectic phase, the liquid crystal textures become significantly altered. The existence of a polymer network not only creates resistance to form a helix and therefore hinders the formation of cholesteric fingerprints but also modifies the structure of the cholesteric texture. We investigate the effects of changing the concentration of chiral dopant and monomer on the formation and growth of the cholesteric fingerprint texture during the phase transition and on the width of the fingerprints. We find that, within a certain parameter range, the cholesteric fingerprints do not depend on the concentration of the chiral dopant. We explain this phenomenon by hypothesizing that the polymer network acts as a bulk alignment field.

DOI: 10.1103/PhysRevE.110.054703

I. INTRODUCTION

For many decades, mixtures of low molar mass liquid crystals (LCs) and polymers have been studied in the context of science and technology. These systems are of great interest because of the complex interplay between the two components, as on the one hand the low molar mass LCs can aid polymers' alignment and on the other hand they are disturbed by the polymeric inclusions [1–3]. Mixtures of polymers and LCs have also been used for novel optical materials [4–8].

One lively area of study is the so-called polymer-dispersed liquid crystals (PDLCs), where a solid polymer network is perfused with LCs [1]. PDLCs have been used, for example, to create bistable "smart" windows where an electric field induces a switch between the scattering disordered state and the transparent ordered state [9].

In PDLCs, the LCs occupy a relatively small volume fraction [1]. On the other hand, small amounts of polymers dispersed in LCs have other functions [10]. Polymer fibers dispersed in LCs can align with them and make alignment visible with electron microscopy, revealing the details of the LC deformations [1]. Previous work has shown that it is possible to remove LCs from these samples and still see the imprinted alignment [11–13], recently also observed in delicate structures such as LC shells [14,15]. The effect of polymers is also very important in the presence of LC topological defects. Guest molecules and nano objects in LCs tend to accumulate in defects, and so do polymers [16–18]. The accumulation of polymers in defects reduces the LC elastic energy, therefore addition of polymers is a common method used to stabilize energetically "expensive" defects such as disclination lines. This method has been especially effective in blue phases, where the presence of polymers has increased the range of stability from less than one degree to several tens of degrees, making blue phases usable in optics and photonics [19,20].

Another use of microstructured materials such as engineered polymers or polymers with special conformation has been in templating LC alignment. Chiral polymers are of particular interest. It was shown for example that a chiral polymer can retain twist and imprint it to nonchiral materials [21,22]. Methods based on polymer networks have been used to transfer chirality from LCs to isotropic liquids.

From all these examples, it is clear that LCs influence the alignment of polymers and are in turn affected by it. Perhaps the most notable example of it is the so-called wash-refilling technique, which has been successful in generating optical filters and other optical materials. This consists of crosslinking a polymer network inside a LC, then washing away the LC and refilling the network with another fluid. Cholesteric LCs for example can have tunable or wider reflection bands when polymerizable mesogens are cross-linked in the cholesteric phase [23,24]. Guo *et al*. have used this technique to prepare a single-layer film reflecting both right- and left-circularly polarized light, by refilling right-handed helical cholesteric LC into prefabricated left-handed polymer networks [5,25]. By employing wash-refilling techniques in a wedge cell, Broer and coworkers achieved reflection of one of the two circularly polarized components over the entire visible spectrum by utilizing a gradient in the pitch of the cholesteric helix [4]. Recently, Li *et al*. have used the unwinding of the cholesteric helix near the smectic transition to create multicolor filters [26].

*Contact author: zzheng20@jhu.edu

†Contact author: serra@sdu.dk

Here, we would like to focus on the effect of the polymer network architecture on LC alignment. We choose a simple system to investigate the effect of a smectic polymer network on a cholesteric LC phase. Both smectic-A and cholesteric phases are characterized by a periodic structure; however, the two phases have major differences. Most notably, (i) the direction of periodicity in the smectic-A phase is along the director, while in cholesteric it is perpendicular to it; (ii) the twist and the bend deformations are incompatible with the layer structure of the smectic phase, while in the cholesteric phase twist is favored. Despite the incompatibility between the two phases, cholesteric phases with a long pitch can transition into a smectic-A* (Sm-A*) phases whose textures are very similar to the achiral smectic-A phase [27].

We can easily tune the pitch in cholesteric LCs with the concentration of chiral dopant [28,29]. We use one of the two phases, the long-pitched Sm-A* phase, to template the architecture of the polymer network and we then study the effect this has on the cholesteric textures as we increase the temperature above the phase transition. We choose to observe one typical cholesteric texture, the fingerprint texture, which forms in cholesteric LCs in cells with homeotropic (perpendicular) anchoring. We show that in certain regimes we can describe the alignment from the polymer network as a bulk alignment field.

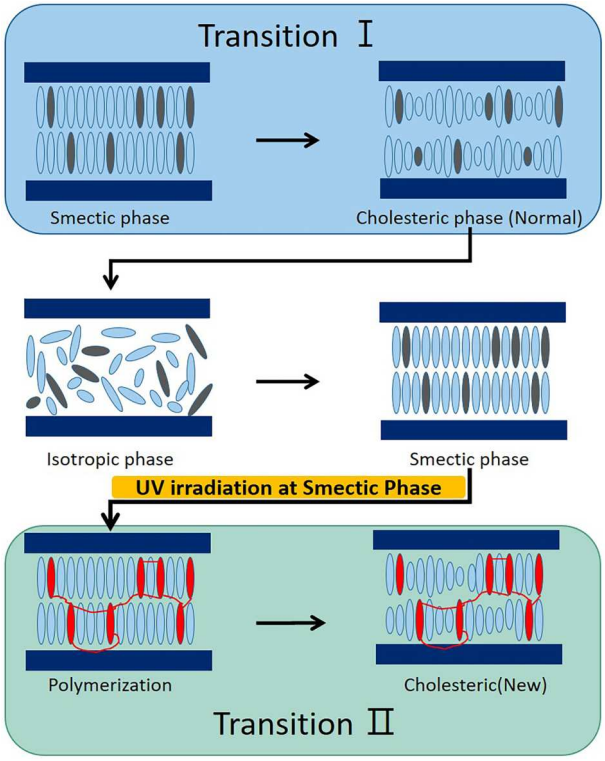

FIG. 1. Schematic of the experiment. In the sketch, we represent the 8CB molecules as light blue ovals and reactive mesogens as dark blue ovals before polymerization and red ovals with links after polymerization. Transition I and transition II are the temperatures at which the cholesteric fingerprints become visible before and after polymerization.

II. MATERIALS AND METHODS

The thermotropic liquid crystal 4-cyano-4'-octylbiphenyl (8CB, Nematel) is mixed with the chiral dopant 4-(2-methylbutyl)-4-cyanobiphenyl (CB15, Nematel), polymerizable monomer 1,4-Bis-[4-(3-acryloyloxypropyloxy) benzoyloxy]-2-methylbenzene (RM257, AmBeed) and photoinitiator 2,2-Dimethoxy-2-phenylacetophenone (DMPA, Sigma-Aldrich).

For the preparation of the sample, we thoroughly clean the glass slides by sonicating them in ethanol, acetone, and isopropanol for 10 min each. In order to impose homeotropic anchoring on the glass surface, the glasses are bathed in a solution of Dimethyloctadecyl[3-(trimethoxysilyl)propyl]ammonium chloride (DMOAP, Sigma-Aldrich) at 3.3% in water for 10 min.

Two pieces of glass are glued with a small amount of epoxy adhesive glue to get a cell with an area of 23 mm × 12 mm. The glue also serves as a spacer, providing a thickness ranging from 5 to 30 μm. We use spectroscopy (Ocean view software in reflecting mode with custom made analyzing Matlab code) to screen cells with average thickness between 10-20 μm. For each cell, there is typically a variation in thickness of 2 μm across the entire cell.

Once we have measured the cell thickness, we introduce a mixture of 8CB, monomer, photoinitiator, and chiral dopant. The mixtures span concentrations of monomer and chiral dopant from 0 to 5 wt % and a fixed concentration of 0.1% photoinitiator. Under yellow light conditions, these mixtures are introduced into sandwich cells in the isotropic phase.

The LC textures are identified by optical microscopy with a temperature control system. The identification is primarily determined through observations using a polarizing optical microscope (POM) Nikon Eclipse LV110N Pol equipped with a DS-Ri2 (Nikon, Tokyo, Japan) camera. The sample is placed on an Instec HCS302 MK 2000 water-cooled heating stage (Instec Inc., Boulder, CO, USA), and various heating and cooling rates are applied. This technique does not accurately capture the smectic-nematic transition when the sample has purely homeotropic anchoring and long cholesteric pitch. However, here we are interested in monitoring the change of texture from the smectic to the cholesteric phase. So our transition does not correspond to a true phase transition, but to the point at which the cholesteric fingerprints appear. In order to measure the real phase transition temperature, we utilize samples with planar anchoring.

With the homeotropic cell, we follow this measurement protocol (Fig. 1): we start with an LC mixture in its isotropic phase, gradually decreasing the temperature to 25°C at a rate of 1°C/min until the system is well in the Sm-A* phase. Subsequently, we increase the temperature of the sample to the cholesteric phase at 35°C at a rate of 0.25°C/min (Transition I) and measure the temperature at which we observe the formation of fingerprints. Following this, the samples are cooled down again and crosslinked while in the Sm-A* phase at 25 °C. The glass cells are subjected to UV irradiation for 10 min (with a wavelength of 365 nm and an emission intensity of 140 mW/cm^2, Hamamatsu lamp L11921), during which the monomer undergoes cross-linking to generate a polymer network. After cross-linking, we perform a temperature ramp

identical to the one carried out prior to cross-linking, bringing the sample back into the cholesteric phase (Transition II) and observing the formation of the texture.

III. RESULTS AND DISCUSSION

We investigate the impact of monomer and chiral dopant concentration on the smectic-cholesteric phase transition in LCs. As detailed in Sec. II, we prepare mixtures with varying concentrations of chiral dopant and reactive mesogen (ranging from 0% to 5%), heat them above clearing temperature, and introduce them into thin glass cells treated for homeotropic anchoring. Each sample is then left to cool down to room temperature. Before polymerization, the sample is reheated into the isotropic phase, cooled down in the smectic phase, and photo-polymerized. After polymerization, the sample is heated again to the cholesteric phase and back (Fig. 1).

During the phase transition from smectic to cholesteric, before polymerization, the arrangement of molecules changes from a layered smectic structure to a chiral texture, a transition that we observe as we view the sample between cross polarizers. The smectic phase appears completely dark, because the LC director is perpendicular to the direction of propagation of the incident light, while in the cholesteric phase we can observe the characteristic fingerprint texture, which indicates that the axes of the cholesteric helices lay on the plane of the LC cell.

We observe that if we vary the temperature very slowly with a heating rate of 0.25 °C/min the fingerprint texture seems to grow as a single front, with the fingerprints growing perpendicular to the front (see Supplemental Video 1 [30]), which matches prior observations [31]. The presence of a single front is most likely due to small temperature gradients across the sample. We verify by varying the amount of chiral dopant that the width of the fingerprints depends on the pitch of the cholesteric helix, as expected (Supplemental Material [30] Sec. 1 and Fig. S1).

If we analyze the temperature at which we observe a transition between the dark texture and the fingerprint texture, we observe a decrease in temperature with the increasing concentration of reactive mesogen and chiral dopant (Supplemental Material [30] Fig. S2). We should remark that we are only observing the onset temperature of the fingerprint texture, and not the real transition temperature.

In addition, we verify that in the absence of polymerizable mesogens, the effect of the chiral dopant is to decrease the phase transition temperature from smectic to cholesteric (Supplemental Material [31] Fig. S3). The same is valid for the addition of polymerizable mesogen, as reported in [14].

After polymerization, we repeat the temperature ramp and observe how the cholesteric phase develops, depending on the concentration of reactive mesogen and chiral dopant.

Based on the LC behavior, we classify all the samples into three different cases (Fig. 2):

(i) For mixtures with a high concentration of chiral dopant but a low density of polymer network (yellow circles in Fig. 2), the polymer network is fragile and can be easily destroyed by the large-scale rearrangement that occurs during the phase transition. The behavior before and after polymerization remains mostly unchanged and we recover the slowly

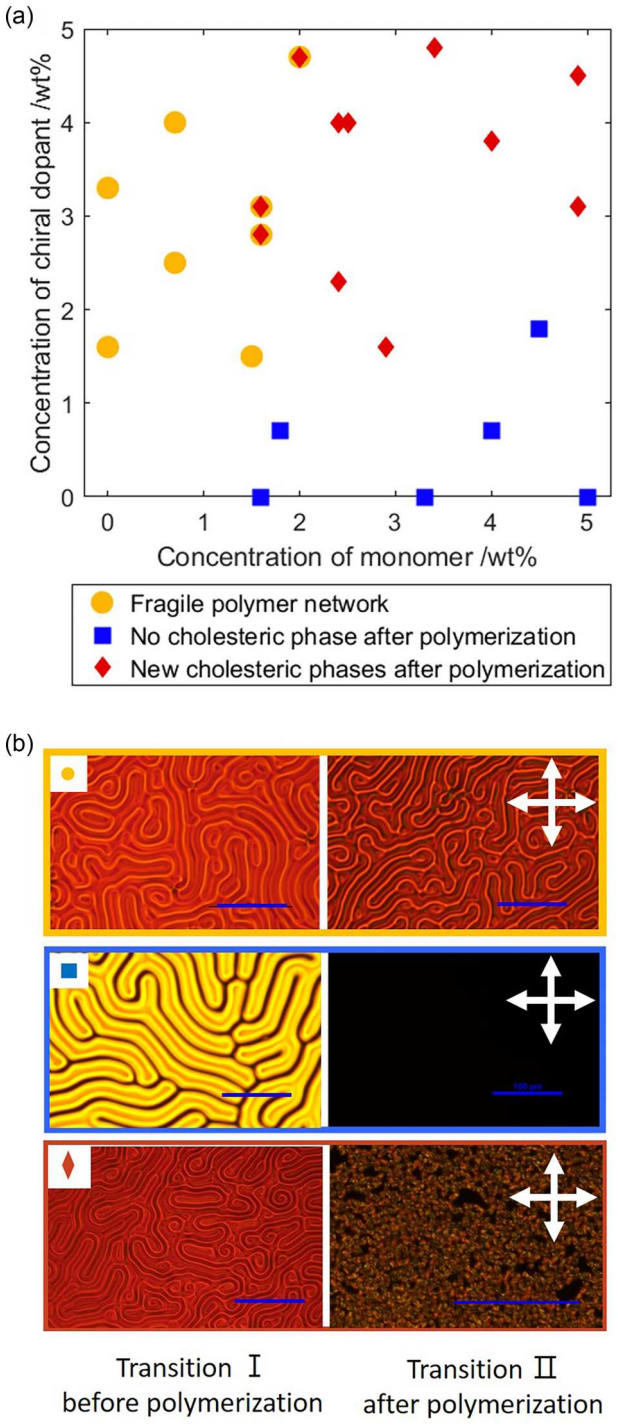

FIG. 2. (a) Classification of data points depicting the diverse behavior of liquid crystal (LC) under varying concentrations of chiral dopant and monomer. Yellow circles indicate that the fingerprint texture is not significantly altered after polymerization. The blue square indicates that no cholesteric phase is visible after polymerization. The red diamonds indicate a different cholesteric texture after polymerization. The data points exhibiting both circles and diamonds indicate an intermediate structure. (b) Representative images of the three types of LC textures before and after polymerization [same color coding as panel (a)]. The white cross double-headed arrow denotes the orientation of the polarizer and analyzer. All scale bars correspond to 100 μm.

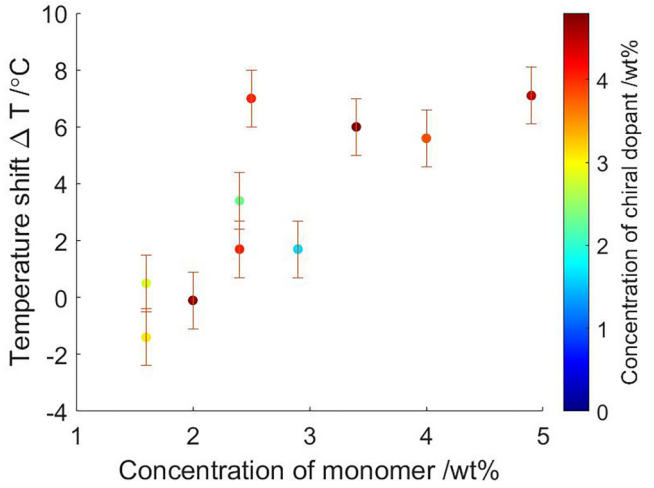

FIG. 3. Temperature shift for the appearance of fingerprint texture after polymerization, plotted with the concentration of monomer. The colors of the points represent the concentration of the chiral dopant in each sample.

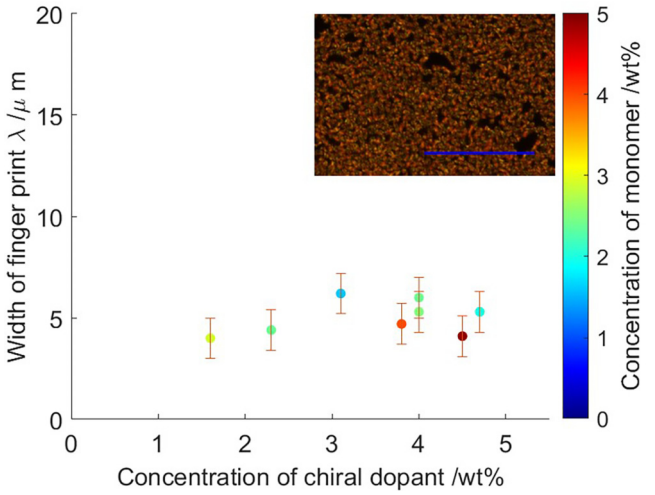

FIG. 4. After polymerization, the width of the fingerprints in samples with relatively high concentrations of chiral dopant and monomer shows almost no dependence on the concentration of chiral dopant. The color bar stands for the different concentrations of the monomer in each sample. The inset shows the cholesteric texture after polymerization, with a scale bar 100 μm.

growing fingerprint texture. We have evidence that the polymer network is broken from small birefringent fragments, visible also in the isotropic phase after polymerization, which appear as debris in the sample and are very likely small bundles of aggregated polymers (Supplemental Material [30] Fig. S4).

(ii) On the opposite end of the diagram, mixtures with high-density polymer networks but low chirality show a different behavior (blue squares in Fig. 2). The LC shows the cholesteric fingerprint texture before polymerization but not after cross-linking. The texture appears dark at all temperatures, indicating that the homeotropic alignment of the polymer network prevents the formation of the fingerprints.

(iii) The most intriguing cases are mixtures with relatively high concentrations of both chiral dopant and monomer. The mixture shows the influence of a smectic polymer network on LC in the cholesteric phase (red diamonds in Fig. 2). Due to the presence of the polymer network, the fingerprint texture is not free to develop homogeneously as before. However, the twist elastic energy penalty is too high for the sample not to twist. The result is a distorted texture with disordered cholesteric fingers that develops from many nucleation points and eventually fills the whole sample.

Finally, we identify a transition region between the unaltered cholesteric texture and the heavily distorted texture (points with both a yellow circle and a red diamond), confirming that indeed the concentration of the reactive mesogen is the relevant parameter that changes the fingerprint texture.

If we now look at the temperature at which the fingerprints appear, the situation is very different from the pre-polymerization case. The shift in this temperature between the pre- and post-polymerization measurements is strongly dependent on the monomer concentration (Fig. 3), showing a large temperature increase for the high concentration of monomer. This indicates that the specific geometry of the smectic polymer network favors the smectic alignment and provides an energy barrier to the onset of the fingerprint texture. The temperature shift is only weakly dependent on the concentration of chiral dopant (color bar in Fig. 3).

We now focus on the samples belonging to the third group (high monomer and high chiral dopant, red diamonds in Fig. 2) and in particular we analyze the width of the new type of fingerprints after polymerization. We should remark that we measure this width during the transition, where individual fingerprints are still clearly distinguishable from each other. With these observations, we find that the fingerprint width is essentially constant (Fig. 4), around 3–6 μm, in contrast with the concentration dependence previously observed. What sets this length scale? Using electron microscopy, we observe the architecture of a polymer network built using the same material and polymerization conditions, and we find an average pore size of roughly 500 nm (see Supplemental Material [30] Sec. 2 and Fig. S5). The average size of the fingerprints, being much bigger, is thus not a measurement of the pore size. Still, it is of the order of the typical values of the extrapolation length of LCs, i.e., the ratio between elastic constant and anchoring strength.

We hypothesize that the weak planar anchoring on the surface of the polymer fibers, integrated over a very large surface, leads to a change in LC alignment. However, it is challenging to estimate the strength of this interaction and the total area of the polymer fibers.

Alternatively, we can consider the polymer network alignment as a bulk alignment, akin to an external field. We therefore rely on prior work on the influence of electric fields on fingerprint textures [32–34] to explain our experimental observations. In this framework, we write the free energy density as

$$f = \tfrac{1}{2}K_1(\nabla \times n)^2 + \tfrac{1}{2}K_2(n \cdot (\nabla \times n) + q_0)^2 + \tfrac{1}{2}K_3(n \times (\nabla \times n))^2 - \tfrac{1}{2}\alpha_P^2 \cos^2\theta. \quad (1)$$

Here n is the nematic director, q_0 is the spontaneous twist angle, K_1, K_2, and K_3 represent the splay, twist, and bend elastic constants, α_P is the parameter that identifies the strength of the interaction between the polymer network and the LC, and θ is the angle between the direction of the aligned polymer fiber and nematic director. The expression is formally identical to the free energy of LCs under an electric field, where our factor α_P^2 replaces the dielectric constant and where the angle between the electric field and the nematic director is replaced by the angle between the nematic director and the orientation of the polymer network. We can thus use the results from [32], which integrates the energy density across a cross-section of the cholesteric finger and minimizes the free energy. The width of the fingerprint λ can then be expressed as

$$\lambda = p\sqrt{CJ/(L + M/C + f(\alpha_P))}, \tag{2}$$

$$f(\alpha_P) = \frac{\alpha_P^2 N d^2}{(2\pi)^2 K_2 C}. \tag{3}$$

Here, the parameters J, L, M, and N are solely dependent on elastic constants and geometric factors [32], without any reliance on the pitch or interaction with the polymer network. $C = d/p$ is the confinement ratio between the thickness of the cell and the helical pitch. A more detailed discussion about these parameters and their estimated values can be found in Sec. 3 of the Supplemental Material [30].

In the limit of low density of polymer network, we have

$$\lambda_{\text{low}\,\alpha_P} \approx p\sqrt{CJ/(L + M/C)}. \tag{4}$$

In this case, the width of the fingerprint strongly depends on the concentration of chiral dopant in the LC mixture.

In the case of a high-density polymer network, however, we can neglect the first term L, which is smaller than the other two terms. In the Supplemental Material [30] (Sec. 4), we discuss this approximation in detail as

$$\lambda_{\text{high}\,\alpha_P} \approx p\sqrt{CJ/(M/C + f(\alpha_P))}. \tag{5}$$

The square root contains a factor C^2, which then cancels the factor p outside the root. We have thus shown that with a high density of polymer network, λ does not depend on the pitch p but on the polymer network interaction strength α_P. Consequently, this eliminates the dependence of the fingerprint width on the chiral dopant concentration, as shown in Fig. 4. Even though we do not know the exact relation between the density of the polymer network and α_P, we can assume that $\alpha_P^2 \propto C_m$, where C_m is the concentration of the reactive mesogen. This hypothesis is based on the idea that the energy term in Eq. (1) is linear in the monomer concentration and that the constant of proportionality between α_P^2 and C_m has the units of energy per molecule. Thus we have

$$\lambda_{\text{high}\,\alpha_P} = \frac{2\pi\sqrt{\frac{JK_2}{N}}}{\sqrt{\alpha_P^2 + \frac{(2\pi)^2 MK_2}{Nd^2}}} = \frac{A}{\sqrt{C_m + B^2}}. \tag{6}$$

Our data allows us to test this hypothesis. By postulating that $\alpha_P^2 = \xi \cdot C_m$, where ξ is an arbitrary constant, then we can fit the data to the Eq. (6) with $A = 2\pi\sqrt{\frac{JK_2}{N}}/\xi^{1/2}$ and $B = 2\pi\sqrt{\frac{MK_2}{Nd^2}}/\xi^{1/2}$. The results, shown in Fig. 5, show that this hypothesis is compatible with the data.

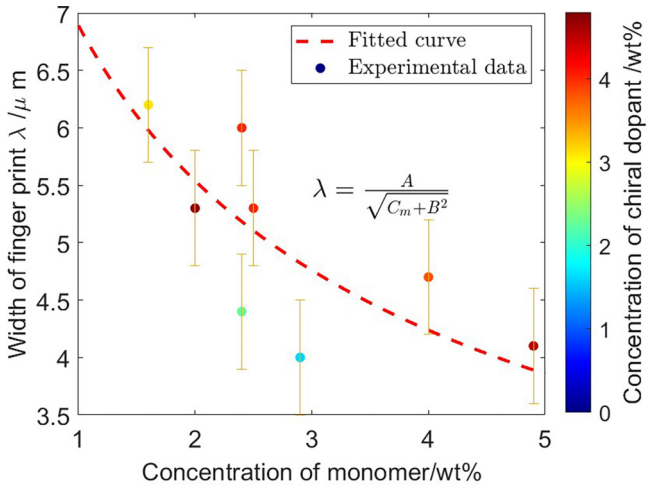

FIG. 5. Width of the fingerprints as a function of monomer concentration. The color of the points indicates the concentration of the chiral dopant. The dotted line represents a fit with two free parameters A and B based on Eq. (6).

IV. CONCLUSIONS

In conclusion, this study investigates the impact of a polymer network with a smectic architecture on the LC cholesteric phase. In particular, we study the effect of the monomer and chiral dopant concentration on the phase transition with and without the polymer network. Through a series of experiments, we observe changes in LC behavior before and after polymerization and identify different cases based on the concentration of chiral dopant and monomer. Our findings indicate that the presence of a polymer network with smectic alignment plays a significant role as an additional energy barrier to the cholesteric fingerprint texture. Additionally, we find that the concentration of the polymer network is a key parameter in determining the width of the cholesteric fingers. Finally, we hypothesize that in certain regimes the smectic network acts as a bulk alignment field akin to an electric field. Overall, this study provides insights into the behavior of liquid crystals-polymer composites and the role of the architecture of the polymer network.

ACKNOWLEDGMENTS

We thank R. Leheny and M. Kim for helpful guidance. This work was supported in part by the National Science Foundation Division of Materials Research (NSF-DMR) under Grant No. 2004532. Any opinions, findings, and conclusions or recommendations expressed in this material are those of the author(s) and do not necessarily reflect the views of the NSF.

Z.Z. designed the research and performed the experiments and the data analysis. F.S. designed and supervised the research and acquired funding. Both authors wrote the paper.

[1] I. Dierking, Polymer network–stabilized liquid crystals, Adv. Mater. **12**, 167 (2000).

[2] D. J. Broer, G. N. Mol, and G. Challa, In-situ photopolymerization of oriented liquid-crystalline acrylates, 5.†. Influence of the alkylene spacer on the properties of the mesogenic monomers and the formation and properties of oriented polymer networks, Die Makromol. Chem. **192**, 59 (1991).

[3] T. Bellini, N. A. Clark, and D. W. Schaefer, Dynamic light scattering study of nematic and smectic-a liquid crystal ordering in silica aerogel, Phys. Rev. Lett. **74**, 2740 (1995).

[4] D. Broer, J. Lub, and G. Mol, Wide-band reflective polarizers from cholesteric polymer networks with a pitch gradient, Nature (London) **378**, 467 (1995).

[5] J. Guo, H. Cao, J. Wei, D. Zhang, F. Liu, G. Pan, D. Zhao, W. He, and H. Yang, Polymer stabilized liquid crystal films reflecting both right-and left-circularly polarized light, Appl. Phys. Lett. **93**, 201901 (2008).

[6] A. Karausta and E. Bukusoglu, Liquid crystal-templated synthesis of mesoporous membranes with predetermined pore alignment, ACS Appl. Mater. Interfaces **10**, 33484 (2018).

[7] Y. Wang, Z.-g. Zheng, H. K. Bisoyi, K. G. Gutierrez-Cuevas, L. Wang, R. S. Zola, and Q. Li, Thermally reversible full color selective reflection in a self-organized helical superstructure enabled by a bent-core oligomesogen exhibiting a twist-bend nematic phase, Mater. Horizons **3**, 442 (2016).

[8] Y.-C. Hsiao, C.-T. Hou, V. Y. Zyryanov, and W. Lee, Multichannel photonic devices based on tristable polymer-stabilized cholesteric textures, Opt. Express **19**, 23952 (2011).

[9] W. Shen and G. Li, Recent progress in liquid crystal-based smart windows: Materials, structures, and design, Laser Photonics Rev. **17**, 2200207 (2023).

[10] J. Y. Han, K. Kim, C. Lee, and D. K. Yoon, Controlled mesoscopic growth of polymeric fibers using liquid crystal template, Macromol. Rapid Commun., 2300303 (2023).

[11] D. J. Broer, H. Finkelmann, and K. Kondo, In-situ photopolymerization of an oriented liquid-crystalline acrylate, Die Makromol. Chem. **189**, 185 (1988).

[12] D. J. Broer, J. Boven, G. N. Mol, and G. Challa, In-situ photopolymerization of oriented liquid-crystalline acrylates, 3†. Oriented polymer networks from a mesogenic diacrylate, Die Makromol. Chem. **190**, 2255 (1989).

[13] J. Guo, H. Wu, F. Chen, L. Zhang, W. He, H. Yang, and J. Wei, Fabrication of multi-pitched photonic structure in cholesteric liquid crystals based on a polymer template with helical structure, J. Mater. Chem. **20**, 4094 (2010).

[14] J. Noh, B. Henx, and J. Lagerwall, Taming liquid crystal self-assembly: The multifaceted response of nematic and smectic shells to polymerization, Adv. Mater. **28**, 10170 (2016).

[15] X. Liu, M.-A. Moradi, T. Bus, J. P. Heuts, M. G. D. Debije, and A. P. Schenning, Monodisperse liquid crystalline polymer shells with programmable alignment and shape prepared by seeded dispersion polymerization, Macromolecules **54**, 6052 (2021).

[16] X. Wang, D. S. Miller, E. Bukusoglu, J. J. de Pablo, and N. L. Abbott, Topological defects in liquid crystals as templates for molecular self-assembly, Nat. Mater. **15**, 106 (2016).

[17] J. X. Velez, Z. Zheng, D. A. Beller, and F. Serra, Emergence and stabilization of transient twisted defect structures in confined achiral liquid crystals at a phase transition, Soft Matter **17**, 3848 (2021).

[18] Y. Luo, F. Serra, D. A. Beller, M. A. Gharbi, N. Li, S. Yang, R. D. Kamien, and K. J. Stebe, Around the corner: Colloidal assembly and wiring in groovy nematic cells, Phys. Rev. E **93**, 032705 (2016).

[19] Z. Zhu, Y. Gao, and J. Lu, Multi-pitch liquid crystal filters with single layer polymer template, Polymers **13**, 2521 (2021).

[20] H. Kikuchi, M. Yokota, Y. Hisakado, H. Yang, and T. Kajiyama, Polymer-stabilized liquid crystal blue phases, Nat. Mater. **1**, 64 (2002).

[21] S. Courty, A. R. Tajbakhsh, and E. M. Terentjev, Chirality transfer and stereoselectivity of imprinted cholesteric networks, Phys. Rev. E **73**, 011803 (2006).

[22] A. Ryabchun, I. Raguzin, J. Stumpe, V. Shibaev, and A. Bobrovsky, Cholesteric polymer scaffolds filled with azobenzene-containing nematic mixture with phototunable optical properties, ACS Appl. Mater. Interfaces **8**, 27227 (2016).

[23] C.-T. Xu, P. Chen, Y.-H. Zhang, X.-Y. Fan, Y.-Q. Lu, and W. Hu, Tunable band-pass optical vortex processor enabled by wash-out-refill chiral superstructures, Appl. Phys. Lett. **118**, 151102 (2021).

[24] D. Zhang, W. Shi, H. Cao, Y. Chen, L. Zhao, P. Gan, Z. Yang, D. Wang, and W. He, Reflective band memory effect of cholesteric polymer networks based on washout/refilling method, Macromol. Chem. Phys. **221**, 1900572 (2020).

[25] J. Guo, H. Yang, R. Li, N. Ji, X. Dong, H. Wu, and J. Wei, Effect of network concentration on the performance of polymer-stabilized cholesteric liquid crystals with a double-handed circularly polarized light reflection band, J. Phys. Chem. C **113**, 16538 (2009).

[26] L. Li, Z.-B. Wen, D. Li, Z.-Y. Xu, L.-Y. Shi, K.-K. Yang, and Y.-Z. Wang, Fabricating freestanding, broadband reflective cholesteric liquid-crystal networks via topological tailoring of the sm–ch phase transition, ACS Appl. Mater. Interfaces **15**, 21425 (2023).

[27] S. M. Hare, B. Lunsford-Poe, M. Kim, and F. Serra, Chiral liquid crystal lenses confined in microchannels, Mater. **13**, 3761 (2020).

[28] P.-G. De Gennes and J. Prost, *The Physics of Liquid Crystals* (Oxford university press, Oxford, UK, 1993).

[29] I. Dierking, Chiral liquid crystals: Structures, phases, effects, Symmetry **6**, 444 (2014).

[30] See Supplemental Material at http://link.aps.org/supplemental/10.1103/PhysRevE.110.054703 for video captions, additional figures and an expanded discussion.

[31] P. Oswald, J. Baudry, and T. Rondepierre, Growth below and above the spinodal limit: The cholesteric-nematic front, Phys. Rev. E **70**, 041702 (2004).

[32] P. Ribiere and P. Oswald, Nucleation and growth of cholesteric fingers under electric field, J. Phys. France **51**, 1703 (1990).

[33] P. Oswald, J. Baudry, and S. Pirkl, Static and dynamic properties of cholesteric fingers in electric field, Phys. Rep. **337**, 67 (2000).

[34] F. Lequeux, P. Oswald, and J. Bechhoefer, Influence of anisotropic elasticity on pattern formation in a cholesteric liquid crystal contained between two plates, Phys. Rev. A **40**, 3974 (1989).